

Application of Harmonic Balance Technique to Synthetic Jets in Cross-Flow

Gerard E. Welch*

Army Research Laboratory, Vehicle Technology Directorate, Cleveland, OH 44135

Ivana M. Milanovic†

University of Hartford, W. Hartford, CT 06117

Khairul B. M. Q. Zaman‡

NASA John H. Glenn Research Center at Lewis Field, Cleveland, OH 44135

The harmonic balance technique was applied to solve the incompressible Navier-Stokes equations for the time-periodic flow fields associated with synthetic jets in quiescent and cross-flows. The method yields approximate time-mean and unsteady flow field solutions through a series of steady-state computations for frequency domain variables. Relatively accurate solutions for the time-mean flow field were obtained using truncated series of low harmonic order (*e.g.*, three to five). Computational results were compared against hotwire data from complementary low-speed wind tunnel experiments with various synthetic-jet slot aspect ratios and jet-to-freestream momentum ratios. The preliminary assessment of the computational methodology suggests that the harmonic balance technique has potential to offer an efficient means by which to simulate forced time-periodic flow fields of interest to the aeropropulsion community.

Nomenclature

b	=	jet half-width at half maximum velocity
D	=	$w\sqrt{4l/(\pi w)}$, effective diameter of slot
f	=	fundamental frequency of forcing function
\underline{F}	=	flux vector, in x-direction (transverse to jet)
\underline{G}	=	flux vector, in y-direction (jetwise)
\underline{H}	=	source-term vector
i	=	$\sqrt{-1}$
J	=	$V_{\max}^2 / U_{\infty}^2$, jet-to-freestream momentum ratio
l	=	slot length
L	=	$V_{\max} \tau$, length scale ("stroke length")
m	=	denotes m^{th} harmonic
M	=	harmonic at which Fourier series is truncated
\underline{Q}	=	vector of unknowns
\underline{r}	=	position vector
Re	=	$V_{\max} L / \nu$, Reynolds number
t	=	time ($time / \tau$)
$\underline{u}(\underline{r}, t)$	=	(u_x, u_y) , instantaneous velocity
U_{∞}	=	freestream velocity
$\underline{U}(\underline{r})$	=	$(U(\underline{r}), V(\underline{r}))$, velocity in frequency domain

* Aerospace Engineer, Engine Components Division, Compressor Branch, Mail Stop 5-10, Senior Member AIAA

† Assistant Professor, Department of Mechanical Engineering, 200 Bloomfield Ave., Member AIAA

‡ Aerospace Engineer, Propulsion Systems Division, Nozzle Branch, Mail Stop 86-7, Associate Fellow AIAA

V_{\max}	=	peak velocity of synthetic jet at orifice
w	=	slot width
x	=	direction transverse to synthetic jet, in direction of freestream
y	=	jetwise direction
z	=	direction normal to x and y

Symbols

α	=	synthetic jet pitch angle (90-degrees herein)
β	=	synthetic jet yaw angle
δ	=	boundary-layer thickness
η	=	fitting coefficient (= 0.88) in collapsed jet profile $V_0 / V_{\max} = \cosh^{-2}(\eta x / b)$
θ	=	boundary-layer momentum thickness
ν	=	kinematic viscosity
ξ	=	boundary-value of jet Fourier coefficient
τ	=	$1/f$ = period of forcing; also used as pseudo time for relaxation solution method
$\psi(\underline{r}, t)$	=	$\sum_m \Psi_m(\underline{r}) \exp(-i2\pi m t)$, stream function
$\omega(\underline{r}, t)$	=	$\sum_m \Omega_m(\underline{r}) \exp(-i2\pi m t)$, scalar vorticity
*	=	denotes complex conjugate

I. Introduction

Active flow-control technologies for aeropropulsion applications are often based on the purposed exploitation of time-periodic, coherent, large-scale vortices to augment entrainment and effective mixing rates in terms of the time-mean flow.¹ The benefits of the augmented time-mean mixing have been used to increase the performance of high lift systems,² to eliminate boundary-layer separation,^{3,4} and to enhance stability.⁵ Direct computational simulation of such unsteady flow fields can be prohibitive in terms of computer time and the volume of numerical data that must be post-processed during the subsequent analysis phase; further, in practice, the aerodynamicist or designer is often interested principally (if not only) in the time-averaged flow field. The time-periodicity of the flow field provides a strong constraint that should be reflected in efficient methods for flow-field observation, measurement, and modeling.

The principal purpose of the work reported herein was to investigate a method—the harmonic balance technique⁶—by which to compute directly the time mean of flow fields in which the influence of time-periodic coherent vortices is of sufficient magnitude to impact the time-mean flow field substantially, while avoiding the often-prohibitive direct, unsteady computation. A number of flow fields meet this description and are of current interest in the aeropropulsion community, including flow fields associated with pulsed ejector systems used for thrust augmentation, boundary layers controlled by oscillatory injection, and quintessentially, flow fields forced by synthetic jets. The synthetic jet in cross-flow is of particular relevance in a number of aeropropulsion flow-control applications and provides an excellent example of a flow field in which time-periodic vortical unsteadiness significantly impacts the time-mean flow field. Indeed in the limit of initially quiescent background flow (zero cross-flow), gradients in the apparent stress field sustained by the coherent time-periodic forcing are solely responsible for the “synthesized” jet—*i.e.*, streaming.

Time-periodic, linear problems (*e.g.*, in acoustics, electromagnetics, and aeroelasticity) are often amenable to solutions based on separation of field variables into space and time functions, for example by expansion in Fourier time-series. Recently, Hall *et al.*⁶ noted that time-periodic nonlinear equations too could be made separable in space and time through a proposed harmonic decomposition. The field variables are expanded in a Fourier time series comprising the dominant frequency of the time-periodic problem and its harmonics. Terms of the same harmonic order are then equated so as to form an infinite series of coupled equations that are space/time separable. The series is truncated at some finite harmonic order as per the accuracy required, resulting in a finite series of transformed, time-independent equations which are solved in the frequency domain. While there does not appear to be a rigorous mathematical basis for equating the harmonics and truncating the series as such, Hall *et al.* obtained accurate solutions to the unsteady Navier-Stokes equations applied to aeroelasticity problems by retaining relatively few harmonics.⁶ This previous success provides strong motivation, in terms of promised computational efficiency, to apply the harmonic balance technique to suitable time-periodic flows—those in which there exists a dominant forcing frequency.

The specific objectives of the research effort reported herein were i.) to develop a method to compute directly the time-mean flow field associated with an unsteady, time-periodic, flow by application of the harmonic balance technique to the Navier-Stokes equations; and, ii.) to show the applicability of the method by comparison of the computed results with hotwire data from a wind tunnel experiment of a synthetic jet in a cross-flow. The incompressible form of the Navier-Stokes equations was chosen specifically a.) to highlight the role of the time-periodic, coherent, vortices, rather than compressibility, in the formation of the residual of the synthetic jet in the time-mean flow field; and b.) to avoid the triple product terms associated with compressibility (cf. Hall *et al.*⁶).

The outline of the paper is as follows: The synthetic jet and its scaling are first reviewed. The formulation of the computational method is then described and example computations involving a normal synthetic jet in a quiescent background flow are shown. The experiment of the synthetic jet in cross-flow is then described and results are presented. Finally, the computational and experimental results are compared in an initial attempt toward code validation.

II. Synthetic Jet and Scaling

A. Synthetic Jet Description

A schematic diagram of a synthetic jet is shown in Fig. 1. Smith and Glezer⁷ have provided an excellent description of the synthetic jet and relevant scaling laws. The periodic displacement of a diaphragm (or piston) located beneath the test surface effects an alternating flow at a slot or an orifice. On an outstroke, the upward displacement of the driver ejects a vortex pair (or a vortex ring in the case of a round orifice) with high directivity due to the cut lines (shear layers) at the slot edges while on the instroke the downward displacement of the driver ingests flow isotropically into the driver chamber.

The time-mean mass flow rate through the slot is necessarily zero; however, the anisotropy of the ingestion and ejection processes leads to a positive flux of time-mean momentum from the slot. As shown in Fig. 2, a jet appears to be “synthesized” out of the coherent unsteadiness of the time-periodic flow field into the time-mean flow field, the phenomenon known as acoustic streaming. The “jet” is unique however; there is no net mass flow rate through the wall and hence the time-mean jetwise velocity at the wall is zero. The velocity increases with distance away from the wall to some maximum from which it then decays in a manner similar to a “steady” jet.⁷ In a time-mean sense, the initial velocity increase is due to acceleration by the Lamb force of the deviation flow, $\underline{u}' \times \underline{\omega}'$.

B. Scaling

The synthetic jet in cross-flow is depicted schematically in Figure 3. Flow approaches the slot with velocity U_∞ and with a boundary-layer thickness determined by upstream conditions. The slot is forced, for example by an enclosed speaker situated below the slot (not depicted), so that the velocity at the slot is oscillatory. In the computational work herein, the slot is assumed to be 2-D (infinite into the page) and the velocity at the slot is prescribed as a sinusoid with frequency $f = 1/\tau$ and amplitude V_{\max} . A plug flow is assumed and neither the portion of the slot below the surface nor the “speaker” plenum are included in the computation; hence, the only scale associated with the slot is its width, w . In the experiment, the slot is driven by a speaker, which sets the maximum velocity and forcing frequency.

Considering the 2-D synthetic jet in cross-flow shown in Fig. 3, the scales considered in the present work were chosen as follows:

Scale	Forcing	Slot	Fluid
Velocity	V_{\max}	-	U_∞
Time	$\tau = 1/f$	-	$\tau = 1/f$
Length	$V_{\max} \tau$	w	$\theta, U_\infty \tau, \sqrt{\nu \tau}$

By considering these relevant scales for the synthetic jet in cross-flow, the Reynolds number, $Re = V_{\max}^2 \tau / \nu$, the “stroke length” to slot-width ratio $L/w = V_{\max} \tau / w$ (cf. formation number of Gharib *et al.*⁸), the momentum ratio, $J = V_{\max}^2 / U_\infty^2$, and the ratio of momentum thickness to slot width, θ/w , were used to characterize the flow field. In the developed computational solver, all lengths are scaled by the stroke length $L = V_{\max} \tau$ and all velocities by the amplitude of forcing, V_{\max} . The Reynolds number, Re , sets the ratio of the stroke length, L , to viscous length,

$\sqrt{\nu\tau}$. The momentum ratio, J , sets the ratio of the maximum jet velocity at the slot to the freestream velocity, and the ratio of the stroke length to slot width is set by L/w . Note that the scales herein are related to Smith and Glezer's scales,⁷ assuming a sinusoidal forcing function at the jet exit, through $L = \pi L_0$ and $V_{\max} = \pi V_0$, so that $\text{Re} = 4 \text{Re}_{l_0}$ and $L/w = 4 \text{Re}_{l_0}/(\pi \text{Re}_{v_0})$, where $\text{Re}_{v_0} = V_0 L_0/\nu$ and $\text{Re}_{l_0} = \pi^2 V_0 L_0/(4\nu)$.

III. Computational Methodology

The computational methodology is based on the application of the harmonic balance technique to solve the incompressible Navier-Stokes equations. While turbulence levels would influence the breakup of the coherent starting vortices ("smoke rings") and trailing shear-layer vortices associated with the forcing of the synthetic jet, the present work is restricted to laminar viscosity. It might be anticipated that the laminar-viscosity assumption might lead to grossly underestimated entrainment levels and jet decay rates; however, the low turbulence intensity is mimicked to some degree by the (artificially) long-lived coherent vortices of the laminar computation.

A. Vorticity / Stream-Function Formulation

The harmonic balance approach is applied to the stream function and vorticity transport formulation of the 2-D, incompressible Navier-Stokes equations

$$\nabla^2 \psi(\underline{r}, t) = \omega(\underline{r}, t) \quad \text{and} \quad \frac{D\omega}{Dt} = \frac{1}{\text{Re}} \nabla^2 \omega \quad (1)$$

where $\omega = \underline{e}_z \cdot \nabla \times \underline{u}$ and $\underline{u} = (-\partial_y \psi, \partial_x \psi)$. After Hall *et al.*⁶, the primitive variables are expanded in complex Fourier series, for example, $\psi(\underline{r}, t) = \sum_m \Psi_m(\underline{r}) e^{-i2\pi m t}$ and $\omega(\underline{r}, t) = \sum_m \Omega_m(\underline{r}) e^{-i2\pi m t}$, where the summation is understood to be over integers from negative infinity to positive infinity. The series are truncated at a harmonic order, M , dictated by the required accuracy. The terms of the same harmonic order are then equated yielding

$$\nabla^2 \Psi_m(\underline{r}) - \Omega_m(\underline{r}) = 0 \quad (2)$$

$$\nabla \cdot \left(\sum_{l=m-M}^M U_{m-l} \Omega_l - \frac{1}{\text{Re}} \nabla \Omega_m \right) - i2\pi m \Omega_m = 0 \quad (3)$$

with summation $m = (0, 1, \dots, M)$, having noted that the Fourier coefficients of the negative harmonics are equal to the complex conjugates of the corresponding positive harmonic (e.g., $\Psi_{-m}(\underline{r}) = \Psi_m^*(\underline{r})$). The local frequency domain velocity components are given by $(U_m(\underline{r}), V_m(\underline{r})) = (-\partial_y \Psi_m, \partial_x \Psi_m)$. A pseudo-time term is introduced for a subsequent relaxation solution scheme, resulting in the series of $2(M+1)$ governing equations (accounting for both the real and imaginary parts of the Fourier coefficients)

$$\frac{\partial \underline{Q}}{\partial \tau} + \frac{\partial \underline{F}}{\partial x} + \frac{\partial \underline{G}}{\partial y} + \underline{H} = 0 \quad (4)$$

where

$$\underline{Q} = [\Psi_0, \Psi_1, \dots, \Psi_M : \Omega_0, \Omega_1, \dots, \Omega_M]^T \quad (5)$$

$$\underline{F} = \begin{bmatrix} \vdots \\ -\frac{\partial \Psi_m}{\partial x} \\ \vdots \\ \sum_{l=m-M}^M U_{m-l} \Omega_l - \frac{1}{\text{Re}} \frac{\partial \Omega_m}{\partial x} \\ \vdots \end{bmatrix} \quad \text{and} \quad \underline{G} = \begin{bmatrix} \vdots \\ -\frac{\partial \Psi_m}{\partial y} \\ \vdots \\ \sum_{l=m-M}^M V_{m-l} \Omega_l - \frac{1}{\text{Re}} \frac{\partial \Omega_m}{\partial y} \\ \vdots \end{bmatrix} \quad (6)$$

and

$$\underline{H} = [\Omega_0, \Omega_1, \dots, \Omega_M : -i2\pi(0, \dots, m\Omega_m, \dots, M\Omega_M)]^T \quad (7)$$

The equations are transformed into generalized curvilinear coordinates to accommodate grid stretching.

B. Time-Integration

The transformed equations are marched simultaneously in a pseudo-time, τ , using MacCormack's method until "steady-state" is converged upon. Local time-stepping was utilized with local time steps set by CFL constraints based on the local velocity magnitude for each harmonic and the diffusion constraint of the stream function equation; that is, ($\Delta t_m \propto \min[\Delta y / \sqrt{\underline{U}_m \cdot \underline{U}_m^*}, \Delta y^2]$). The resulting time-steps were small and tens of thousands of time-steps were required for convergence of the $2(M+1)$ equations into steady-state in pseudo-time. The apparent stiffness of the equation set would seem to obviate the potential benefit of the harmonic decomposition. However, the small time-steps are attributed to the use of the compressible NS-type solution approach on the incompressible N-S formulation: the time-steps in low velocity regions are set by diffusion rates of the stream function equation which are orders of magnitudes higher than the diffusion rates of the vorticity transport equation.

As indicated, only the eigenfunctions of the zeroth and positive harmonics are computed. The time-mean flow field is obtained directly and is simply the real part of the eigenfunctions of the zeroth-harmonic; similarly, the unsteady flow field is obtained directly via the Fourier series, given the complex eigenfunctions just computed. The solution methodology yields an M -harmonic approximation of the unsteady and time-mean flow fields, while avoiding the direct unsteady computation with its associated post-processing. In calculations to date, the sensitivity to the order of harmonics retained has been assessed by varying M between one, three, and five. Comparisons of the computed flow fields for synthetic jets in quiescent flow show that the dominant features of the synthetic jet—*i.e.*, the large starting vortices—are captured well by low harmonic orders (even one); in some cases a meaningful time-periodic unsteady flow field solution can be obtained with effectively four "steady-state" solutions for the zeroth- and first-harmonic functions.

C. Boundary Conditions

1. Quiescent background

In the case of the 2-D normal synthetic jet in a quiescent background flow, the infinite half-space is artificially truncated at $y/L = 1$ in the jetwise direction and $x/w = 0.5$. Symmetry about the centerline is imposed explicitly at $x = 0$. The lower wall comprises the half-slot region ($0 < x/L < w/2$) and a no-slip surface ($x/L > w/2$). For the study herein, a plug flow is assumed in the slot region; hence, the vorticity in the slot is set to zero and stream function varies linearly according to $\Psi_m = \xi_m^* x$ from zero at the centerline to a maximum value at the slot edge, given $\xi_{m \neq 1} = 0 + 0i$; $\xi_{m=1} = \frac{1}{2} + 0i$. At the no-slip wall the stream function is fixed at the slot-edge value, and the vorticity is obtained by Taylor series expansion, $\Omega_m(1) = 2(\Psi_m(\Delta y) - \Psi_m(0)) / \Delta y^2$ (cf. Roache⁹). At $y/L = 1$, an inflow/outflow boundary, the jetwise derivatives of the vorticity and stream function are set to zero to first and second order, respectively. Finally, at $x/L = 0.5$, generally an inflow plane, the vorticity is set to zero and the stream function is set to the value at the lower wall plus a residual inferred from the interior according to

$$\Psi(\frac{1}{2}, y) = \Psi(\frac{1}{2}, 0) + \frac{1}{\Delta x} \int_0^y \int_0^{y-\Delta y} RES(\frac{1}{2}, y) dy dy, \text{ where } RES(\frac{1}{2}, y) = \frac{1}{4}[5\Psi(\frac{1}{2}, y) - 10\Psi(\frac{1}{2} - \Delta x, y) + 7\Psi(\frac{1}{2} - 2\Delta x, y) - 2\Psi(\frac{1}{2} - 3\Delta x, y)].$$

The approach yielded a stable implementation for physically realizable boundary conditions.

2. Jet in cross-flow

In the case of the normal synthetic jet in cross-flow, the upstream inflow boundary condition was set at a uniform freestream velocity, $\underline{U}_{m,\infty} = (V_m \max/\sqrt{J}, 0)$, so as to set a jet-to-freestream ratio, J , which was varied parametrically. At the inflow plane, the local velocity, vorticity, and stream function are set using an assumed laminar flow model profile, $U_0(y)/U_{0,\infty} = (2y/\delta - y^2/\delta^2)$. The outflow boundary is set by first-order extrapolation of the stream function and vorticity variables from the interior. The boundary conditions for the bottom wall are the same as those for the synthetic jet in quiescent flow mentioned above. The top boundary is an inviscid, impermeable surface on which the stream function is a constant and the vorticity is zero.

D. Results for Synthetic Jet in Quiescent Flow

The computational method was applied to analyze normal synthetic jets in initially quiescent flow over a range of Reynolds numbers from 720 to 72,000 at an L/w of 51. The range was intended to include $Re = 72,000$ and $L/w = 60$, which corresponds to the baseline values ($Re_{U_0} = 18,124$ and $Re_{U_0} = 383$) of Smith and Glezer.⁷ The difference between L/w of 51 versus 60 (experiment) is expected to be insignificant and was caused by a computational slot-width dictated by the grid resolution. The computation was carried out on a stretched 51 x 71 grid in which points are clustered near the jet centerline and slot and near the lower wall where the grid spacing is x/L and $y/L = 7E-4$. The grid spanned $0 < x/L < 0.5$ and $0 < y/L < 1.0$. It is noted that convergence on this grid was not achieved at the $Re = 72,000$ level ($\sqrt{v\tau}/L = 1/\sqrt{Re} = 3.7E-3$). The lack of convergence was manifested as a zeroth-harmonic solution which itself was in a limit cycle rather than an asymptotic steady-state in the pseudo-time. A finer 101 x 101 stretched grid was used with minimum y/L spacing at the $5E-4$ level; however, again a converged solution was not obtained. The cases below concentrate on $Re = 7,200$ ($\sqrt{v\tau}/L = 1.2E-2$) and $L/w = 51$ ($Re_{U_0} = 1,800$ and $Re_{U_0} = 45$) for which converged solutions were attained.

The sensitivity of the solution to the maximum harmonic order, M , was assessed parametrically by varying M over 1, 3, and 5. The typical harmonic power content is evident in Fig. 4 in which the magnitudes of the real part of the zeroth and positive harmonics are plotted. The magnitude of each constituent except the fundamental initially increases in the region from $0 < y/w < 8$ —the point at which the zeroth harmonic (time-mean) velocity peaks (cf. frequency analysis by Smith and Glezer⁷). The constituent magnitudes then decay spatially with a rate seemingly proportional to their harmonic number (in the manner of the eigenfunctions in the classical Stokes oscillating plate).

An example time-averaged (zeroth-harmonic) solution for a normal synthetic jet in initially quiescent flow, computed using with $M = 3$, $Re = 7,200$ and $L/w = 51$, was shown earlier in Fig. 2. Computed values of centerline time-mean jetwise velocity as a function of y/w , for $M = 1, 3$, and 5, are compared with experimental data in Fig. 5. A general observation in the study to date is that the salient features of the synthetic jet—principally the starting vortices (smoke ring) generated during the outstroke and the time-mean jet (streaming)—were qualitatively captured with few harmonics—even $M = 1$. Comparison of computed results (Fig. 5) show that the computed time-mean flow fields of the various harmonic orders are virtually indistinguishable at jetwise distances beyond $y/w = 10$. Note too that the maximum in the centerline time-mean velocity is invariant beyond $M = 3$ and that even the $M = 1$ solution is in qualitative agreement with the high-order computations. The predicted time-mean velocities are larger than the experimental data; however, there is good qualitative agreement in trend including the location of the maxima. It is possible that differences in the experiment and computation introduced by plug-flow assumption at the orifice might be responsible for a mismatch in injected kinetic energy (circulation), which could explain the discrepancy in the magnitude of the scaled time-mean velocity ($V_0(0, y)/V_{max}$).

Smith and Glezer⁷ noted earlier that the distributions of time-mean jetwise and cross-stream velocity compared well with turbulent jet data, even though the synthesized jet is a time-mean residual of time-periodic motion. Further, the transverse profile of jetwise velocity collapsed onto one profile which could be fitted well by a hyperbolic cosine function $V_0/V_{max} = \cosh^{-2}(\eta x/b)$, where η is a fitting coefficient and b is the jet half-width. The computed time-mean jetwise velocity profiles ($Re = 7,200$, $L/w = 51$, $M = 3$) shown in Fig. 6 are compared with the hyperbolic cosine function, using $\eta = 0.88$ determined by best-fit to the computational data, and with the experimental data of Smith and Glezer⁷. A comparison (not shown herein) of the profiles for the $M = 1, 3$, and 5 at $y/w = 26.5$ showed that the solutions are essentially indistinguishable in the similarity region of the jet. It is clear from Fig. 6 that the computed velocity profiles collapse excellently and are in good agreement with experimental results, in spite of the assumed laminar viscosity in the computation. Note that there is a consistent overshoot at one point in the vicinity of the jet centerline, the origin of which remains unclear.

The evolution of the jet width and time-mean centerline velocity are compared on log-log scales in Fig. 7. Also shown are the suggested best-fits for the similarity regions of the jet. Using the computational values, the similarity portion of the jet ($y/w > 25$) are well described by $b(y)/w \propto (y/w)^\eta$ and $V_0(y)/V_{max} \propto (y/w)^{-\eta/2}$, where $\eta = 0.88$ is the coefficient from the hyperbolic cosine function obtained earlier. It is interesting to note that the evolution of the jet width is thus found to be in agreement with Smith and Glezer's experimental findings, in spite of the lack of turbulence modeling in the present study. On the other hand, the decay of the time-mean centerline velocity is slower ($V_0 \propto y^{-0.44}$) in the computational study than that ($V_0 \propto y^{-0.58}$) in the experiment.⁷

The comparisons of the time-mean jet characteristics shown above indicate that the computational methodology yields qualitatively accurate results for the normal synthetic jets in terms of the time-mean flow field. Careful analysis of the unsteady flow field characteristics and correlations remains for future study. The experiment

described in the next section has yielded data that can be used for such future analysis for synthetic jets in cross flows.

IV. Experiment for Slotted Synthetic Jet in Cross-Flow

A. Experiment Description

The normal synthetic jet in a cross-flow was evaluated experimentally in the low-speed open-loop wind tunnel with a 30 inch x 20 inch test section shown in Fig. 8a. The experimental setup was described in detail in an earlier paper.¹⁰ The synthetic jet actuator comprised the speaker in a box mounted beneath the tunnel surface (as shown in Fig. 8b) and a circular cover plate with machined slots as shown in Fig. 9. The speaker is operated at frequencies near the Helmholtz resonance of the configuration, approximately 30 Hz. Typical tunnel free stream velocities are near 20 ft/s. The flow was determined to be turbulent by boundary-layer measurements obtained $5D$ upstream of the slot.

The machined cover plate accommodated four slot geometries, constituting three different aspect ratios ($l:w$) of 4:1, 8:1, and 16:1 and two pitch angles. The slots were designed to have constant exit area with equivalent diameter $D = 0.75$ in., as used in the earlier round synthetic jet experiments.^{11,12} The slots considered in the current study were normal to the tunnel wall (90-degree pitch angle). Yaw angles of ninety degrees (slot orientated with the long end normal to the flow) and zero degrees (long end parallel to the flow) were assessed.

Instantaneous velocity components were measured using hotwire anemometry. Two independent cross-wires set in $u-v$ and $u-w$ orientations were used to sequentially map all three components of instantaneous velocity. Time-mean components, phase-averaged components, and turbulence intensity and velocity correlations were then constructed from the measurements. A single element wire was used to characterize the velocity at the exit of the jet slot.

B. Experimental results

Velocity was measured for the three slot configurations ($l:w = 4:1, 8:1, \text{ and } 16:1$), at three momentum ratios ($J = 1, 5.4, \text{ and } 15.6$), with the slots oriented normal to the flow (ninety-degree yaw angle). In addition, the series were repeated at zero degree yaw angle (slot parallel to the flow) for the 8:1 aspect ratio slot. Example results are shown in Figures 10-12. The time-mean velocity, streamwise vorticity, and turbulence intensity for the 8:1 slot at $J = 5.4$ in ninety- and zero-degree yaw are compared in Figure 10. In the case of the slot normal to the flow, the slot extends (lengthwise) between $-1.25 < z/D < 1.25$ ($-4 < z/w < 4$). The thinning of the boundary-layer in the vicinity of the slot region is evident by comparison with the boundary layer thickness at the extremes of the picture (e.g., for $z/D > 1.5$). Note too that the jet plume is not quite symmetric about the centerline of the slot in the views shown.

V. Simulations of Synthetic Jet in Cross-Flow

A. Time-mean flow

Initial 2-D computations of the synthetic jet in cross-flow were run at $L/w = 51$, $Re = 7,200$, and various M and J . The laminar flow was assumed to have zero boundary-layer thickness at the entrance of the computational domain. The estimated boundary-layer thickness at the slot in the event of no forcing (Blasius equilibrium flow) would be $\delta/L = 2E-3$ (or $\delta/w = 0.1$) and $\sqrt{v\tau}/L = 1.18E-2$ (or $\sqrt{v\tau}/w = 0.6$). The 101 x 71 stretched grid spanned $-3 < x/L < 3$ and $0 < y/L < 3$. An example of the near-slot time-mean flow with $J = 4$ and $M = 1$ is provided in Fig. 13. In the time-mean, the synthesized jet presents a blockage to the freestream which effects a separation/reattachment zone behind the slot. The sequential suction and ejection at the slot surface is evident in movies of field variables reconstructed from the Fourier series solution.

B. Preliminary Validation Case

Limited assessment of the computational method against the wind tunnel data has been carried out to date. The case considered was the 8:1 slot with ninety-degree yaw (slot-length normal to the flow, see Fig. 12). The scaled parameters for the experimental conditions simulated were $J = 1$, $L/w = 34.5$, $Re = 88,000$ ($\sqrt{v\tau}/L = 3.4E-3$), and $\theta/w = 0.22$ at a measurement station located $5D$ upstream of the slot. In the laminar computation, the inlet boundary-layer was set such that the computed θ/w ratio equaled the measured value. The computation was carried out at $M = 1, 3, \text{ and } 5$, on two different domains: i.) a 101 x 101 stretched fine grid with ten near-wall points within the $\sqrt{v\tau}/L$ set by the Reynolds number, spanning $-2 < x/L < 2$ and $0 < y/L < 1$; and, ii.) a relatively coarse 101 x 71 grid spanning $-3 < x/L < 3$ and $0 < y/L < 3$.

The time-mean total velocity field (x - y view at $z = 0$) obtained in the experiment is shown in Fig. 14a. Figures 12a and 14a (and phase-locked pictures not shown here) indicate that $J = 1$ synthetic jet substantially modified the time-mean and unsteady flow fields over the slot centerline ($z = 0$) out to $y/L = 0.2$ ($y/D = 2$, $y/w = 6.4$).

Unfortunately, large discrepancies between the computed and experimental flow fields were found for the $J = 1$ case considered to date. Firstly, convergence was not attained at the $Re = 88,000$ level, independent of the grid resolution and M . At $Re = 8,800$, computations on the finer grid (which substantially resolved the $\sqrt{\nu\tau}$ length scale), would at first converge to a flow field that promised good qualitative agreement with data but would then ultimately diverge as the entire boundary-layer would develop reversed flow near the wall. This occurred independent of M and its cause was not diagnosed. Converged solutions were obtained on the coarser grid at the $Re = 8,800$ level, for all M . While qualitatively similar near the slot, the computational results to date have not reproduced the time-mean nor unsteady flow fields in terms of distances over which the synthetic jet influences the flow field. The computed jet is effectively much weaker than that of the experiment at $J = 1$ and does not influence the time-mean flow field much beyond the boundary-layer height (*e.g.*, $y/L = 0.05$ to 0.1).

The computed time-mean streamwise velocity for $J = 4$, $M = 1$, and $Re = 7,200$ (of Fig. 13) is shown in Fig. 14b. It is evident that the computation at the higher momentum ratio exhibits the qualitative features of the time-mean flow field of the $J = 1$ experiment. In addition to the substantially different momentum ratio, quantitative discrepancies can be attributed to the assumption of laminar flow in the computation, differences between the relative height of the incoming boundary layers to the slot widths in the computation and experiment, asymmetries in the time-mean flow field about the slot centerline (*cf.* Figure 12), and 3-D relief not captured in the 2-D computation.

VI. Discussion

The primary intent of this research was to conduct an initial assessment of the applicability of the harmonic balance technique to simulate nonlinear time-periodic flows, like those associated with the synthetic jet in cross-flow. A number of observations were made during the course of the work:

First, the features of the time-mean flow associated with the normal synthetic jet in quiescent flow—for example, the jetwise evolution of the synthesized jet, its similarity, decay, and scaling—were reproduced well. This was achieved with few (*e.g.*, three) harmonics in the regions beyond ten slot widths from the slot. While the near slot details might be missed, the correct time-mean momentum and qualitatively correct large scale vortices and their induced decay rates were largely captured, even with one harmonic ($M = 1$).

Second, the particular implementation of the harmonic balance technique adopted in this study was found to be extremely slow in terms of the rate of convergence. It is suggested that this results from the very low pseudo-time step sizes that must be taken for the incompressible flow case using the particular time-marching approach adopted herein and is not inherent to the harmonic balance method. It might be inferred that direct unsteady simulation using the same stream-function/vorticity transport formulation would take much longer; however, this conjecture is not supported in this work. The reader is referred to the work of Thomas *et al.*¹² and their compressible Euler implementation of the harmonic balance technique which attains convergence times commensurate with multiple steady-state computations.

Finally, there was a consistent inability to simulate the relatively high experimental Reynolds numbers with the laminar formulation. It is not clear at this time whether this is the true flow physics trying to emerge through the forced time-periodic laminar flow or an inherent problem with the implementation of the harmonic balance technique.

VII. Summary

A computational method based on the harmonic balance technique developed to solve the vorticity-transport/stream-function formulation of the two-dimensional, incompressible Navier-Stokes equations was described. The methodology was applied to compute the unsteady and time-mean flow fields associated with a normal synthetic jet in cross-flow, a prototypical nonlinear problem of key importance to flow control applications. Relatively accurate time-mean flow fields were computed for a synthetic jet in a quiescent background with less than three harmonics; indeed, the time-mean flow from the one-harmonic computations were indistinguishable from higher order computations (three and five) at distances more than ten slot-widths away from the jet. In the one-harmonic case, the approximate unsteady and time-mean flow fields are thus obtained directly from four “steady-state” computations, two each for the complex eigenfunctions of the zeroth- and first-order harmonics.

The computational work was complemented by experimental work in a low-speed wind tunnel. Hotwire data were obtained for a number of slot aspect ratios, slot-orientations relative to the flow, and momentum ratios. The data set for the slot geometries has complemented an earlier set of data for synthetic jets with round holes. A

preliminary validation attempt for a momentum ratio of unity indicated that the impact of the synthetic jet was under-predicted by the computation. Good qualitative agreement between the computed and experimental time-mean flow fields was obtained when the momentum ratio of the computation was increased by a factor of four.

The successful computation of the synthetic jet in the quiescent background to some degree validates the computational methodology and highlights the role of coherent vorticity, and the relative lack of importance of compressibility, in establishing the time-mean flow. While the reported computational approach for the incompressible N-S formulation required long times for convergence into steady-state, the success leads to the conclusion that the harmonic balance approach for simulating nonlinear, time-periodic flow fields of interest to the aer propulsion community is well worthy of further research.

Acknowledgment

This work was funded by an Army Research Laboratory FY03 Director's Research Initiative award (see *Compendium of FY03 DRI Final Reports*, Army Research Laboratory, Jan. 2004, pp. 191-203). This support is gratefully acknowledged.

References

- ¹Ho, C-M., "An Alternate Look at the Unsteady Separation Phenomenon," ed., Krothapalli, A. and Smith, C. A., *Recent Advances in Aerodynamics*, Aug. 1983.
- ²Wynanski, I., "On Active Flow Control—A Personal Perspective," Israel Annual Conference on Aerospace Sciences," Tel Aviv, Feb., 1999.
- ³Seifert, A. and Pack, L. G., "Oscillatory Excitation of Unsteady Compressible Flow over Airfoils at Flight Reynolds Numbers," AIAA-99-0925, Jan, 1999.
- ⁴McCormick, D. C., "Boundary Layer Separation Control with Directed Synthetic Jets," AIAA-00-0519, Jan., 2000.
- ⁵Lorber, P. F., McCormick, D. C., Anderson, T. J., Pollack, M. J., Corke, T. C., and Breuer, K., "Rotorcraft Retreating Blade Stall Control," AIAA-2000-2475, June, 2000.
- ⁶Hall, K. C., Thomas, J. P., Clark, W. S., "Computation of Unsteady Nonlinear Flows in Cascades using a Harmonic Balance Technique," *AIAA J.*, **40** (5), May, 2002, pp. 879-886.
- ⁷Smith, B. L. and Glezer, A., "The Formation and Evolution of Synthetic Jets," *Phys. Fluids*, **10** (9), Sept. 1998, pp. 2281-2297.
- ⁸Gharib, M., Rambod, E., and Shariff, K. (1998) "A Universal Time Scale for Vortex Ring Formation," *J. Fluid Mechanics*, **360**, pp. 121-140.
- ⁹Roache, P. J., *Computational Fluid Dynamics*, Hermosa Publishers, USA, 1982, p. 141.
- ¹⁰Zaman, K. B. M. Q. and Milanovic, I. M., "Synthetic Jets in Cross-Flow. Part 1—Round Jet," AIAA-2003-3714, June, 2003.
- ¹¹Milanovic, I. M. and Zaman, K. B. M. Q., "Synthetic Jets in Cross-Flow, Part 2—Jets from Orifices of Different Geometry," AIAA-2003-3715, June, 2003.
- ¹²Thomas, J. P., Dowell, E. H., Hall, K. C., "A Harmonic Balance Approach for Modeling Three-Dimensional Nonlinear Unsteady Aerodynamics and Aeroelasticity, IMECE-2002-32532, Nov., 2002.

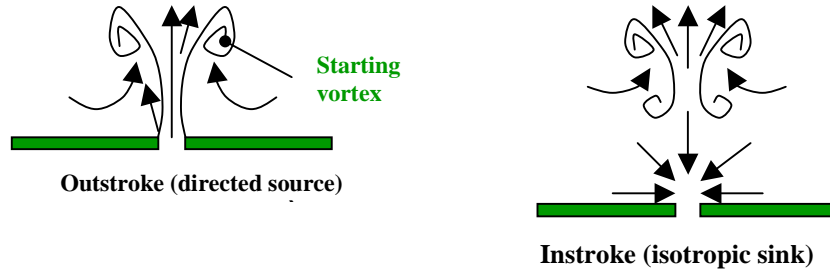


Figure 1. Schematic diagrams depicting the instroke and outstroke of a normal synthetic jet into an initially quiescent background.

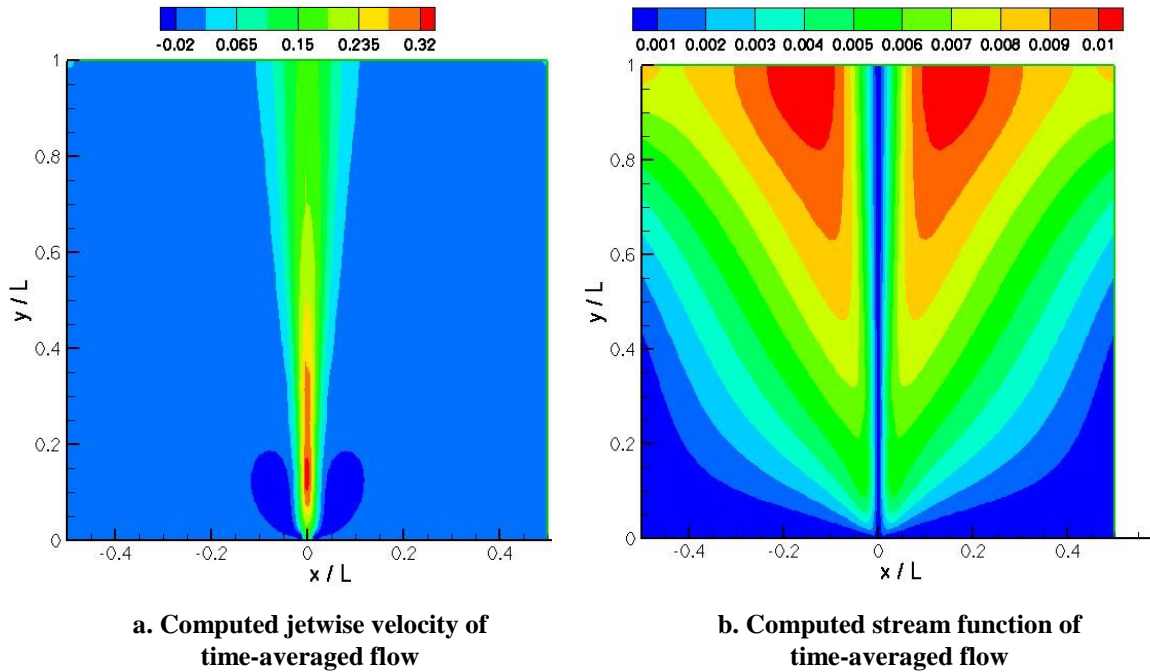


Figure 2. Computed contours of time-averaged (zeroth-harmonic) a.) velocity and b.) stream function of the “synthesized jet” ($M = 3$ at $Re = 7,200$ and $L/w = 51$).

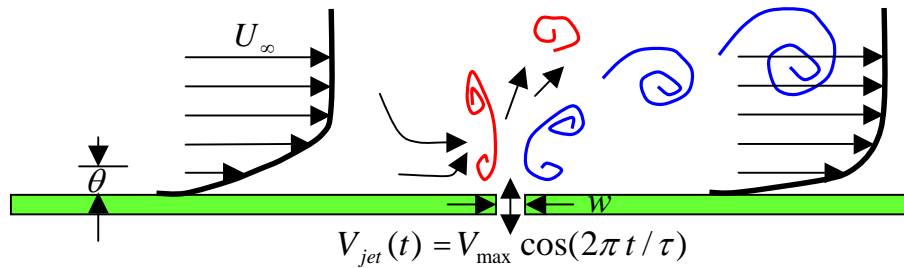


Figure 3. Schematic diagram of a normal synthetic jet in cross flow, indicating some of the relevant length, velocity, and time scales.

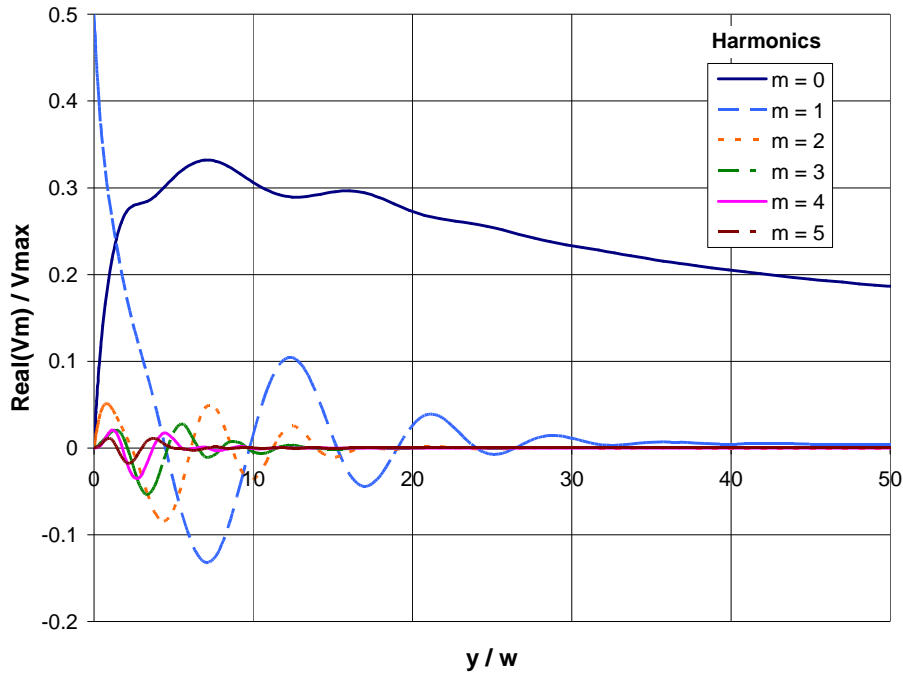


Figure 4. Centerline jetwise-velocity harmonic constituents from a computation of normal synthetic jet in quiescent flow ($M = 5$, $Re = 7,200$, $L/w = 51$).

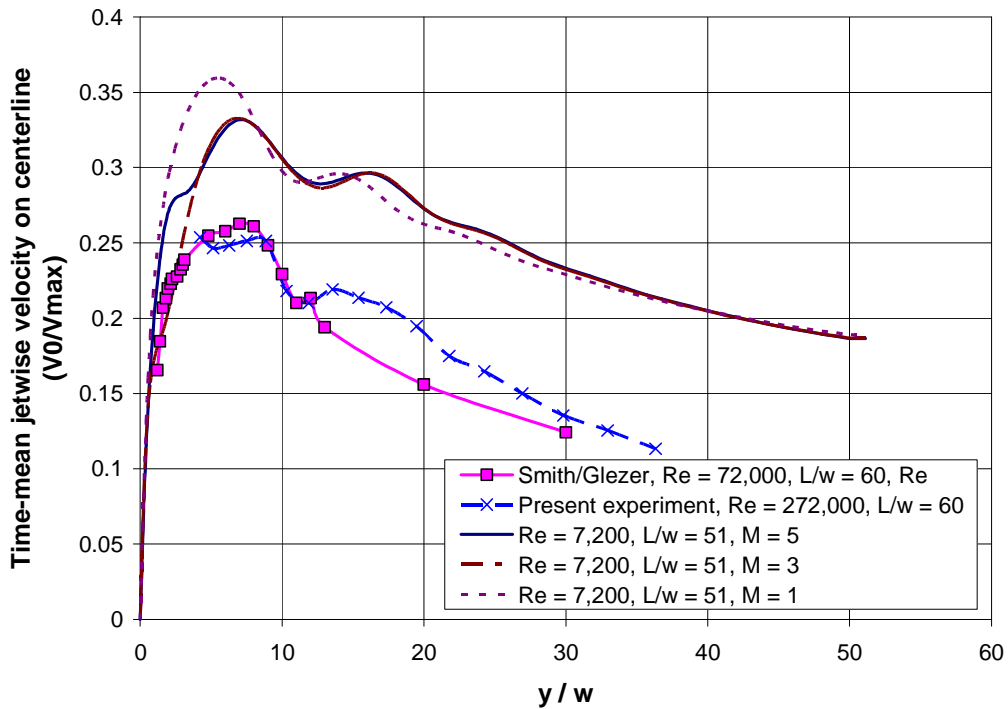


Figure 5. Comparison of computed and experimental time-mean jetwise velocity at the centerline ($x/w = 0$). The experiments were carried out at $L/w = 60$ and $Re = 72,000$ (Smith and Glezer⁷), $L/w = 60$ and $Re = 272,000$ (present experiment), and the computations at $L/w = 51$ and $Re = 7,200$ for $M = 1, 3$, and 5 .

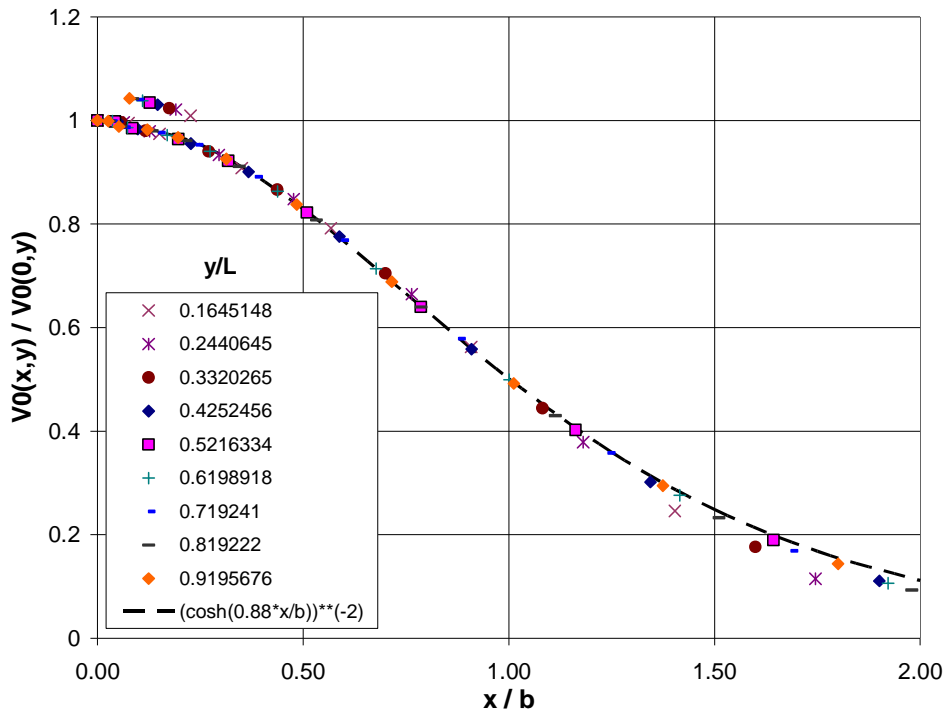


Figure 6. Normalized computed velocity profiles at various y/L for $Re = 7,200$, $L/w = 51$, and $M = 3$ compared with curve fit representing the mean values from data from Smith and Glezer⁷. (Note, Smith and Glezer curve shifted by $x/b = 0.08$ to account for offset in their jet centerline.)

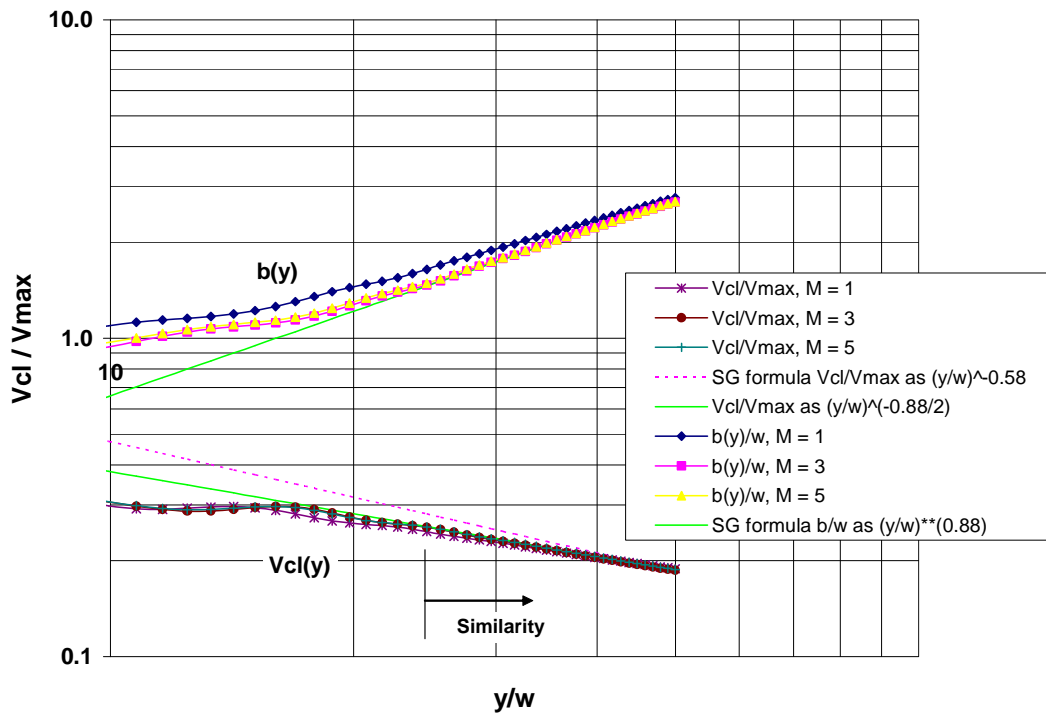


Figure 7. Comparison of computed values of jet half-width and time-mean centerline velocity as a function of jetwise position (for $M = 1, 3$, and 5) with similarity scaling from Smith and Glezer⁷ (SG) and best fit.



a. Perspective view of open-loop low-speed wind tunnel



b. Test Section, showing housing of woofer that drives SJ

Figure 8. Picture of a.) the low-speed wind tunnel and b.) test section with attached speaker-box containing the woofer that drives the synthetic jet.

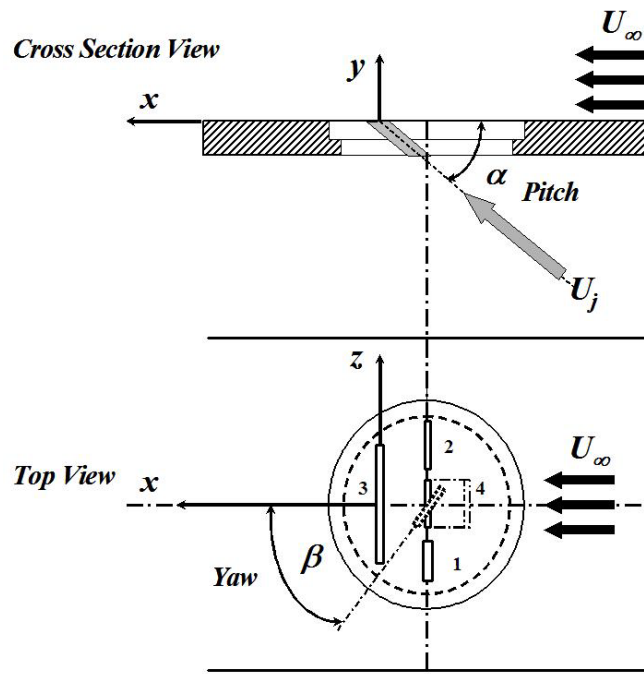


Figure 9. Side and top views of machined cover plate containing the various synthetic jet slot geometries and indicating pitch and yaw angle definitions.

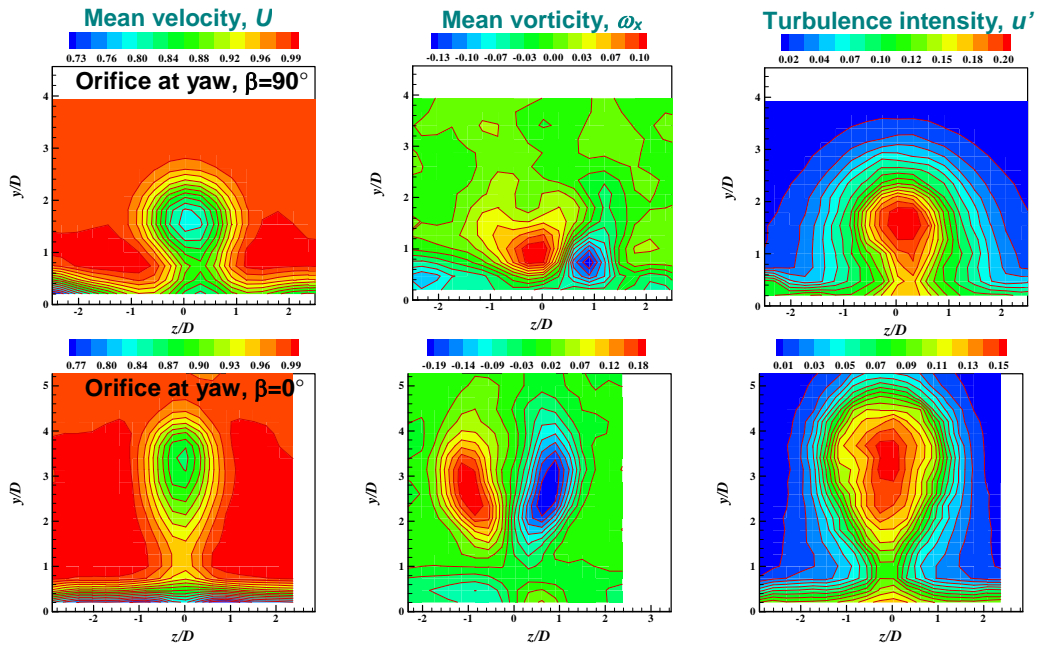


Figure 10. Example experimental data for normal synthetic jets in cross-flows, showing time-mean velocity, streamwise-vorticity, and turbulence intensity as measured at a plane $x/w = 16$ ($x/D = 5$) downstream from 8:1 slots set at two yaw angles (normal to flow and parallel to flow) for momentum ratio $J = 5.4$. The observer is looking upstream in this view.

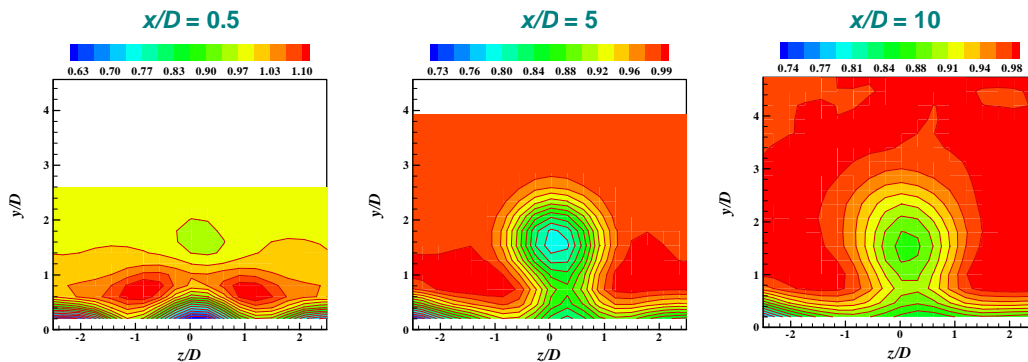


Figure 11. Contours time-mean velocity showing evolution of synthesized jet in cross-flow at various positions downstream of 8:1 slot set at 90-degree yaw angle (normal to flow) for momentum ratio $J = 5.4$. The observer is looking upstream in this view. Note that jet is not quite symmetric about centerline.

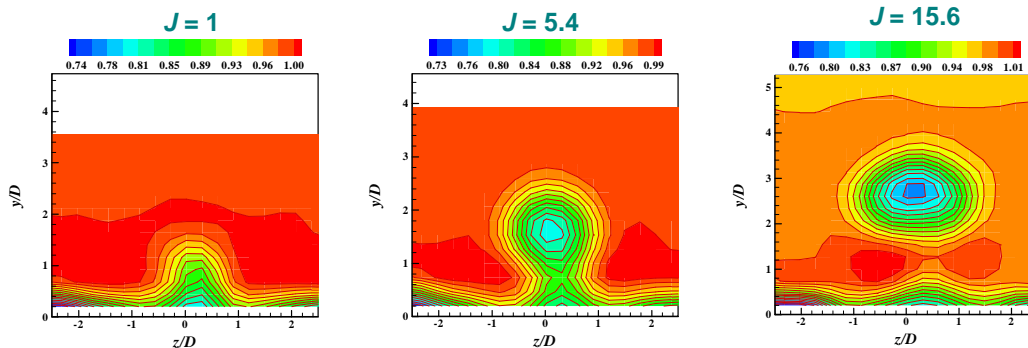


Figure 12. Contours of time-mean velocity at fixed location, $x/D = 5$ ($x/w = 16$), downstream of 8:1 slot set at 90-degree yaw angle (normal to flow) for various momentum ratios, $J = 1, 5.4,$ and 15.6 . The observer is looking upstream in this view. Note that jets are not symmetric about the centerline.

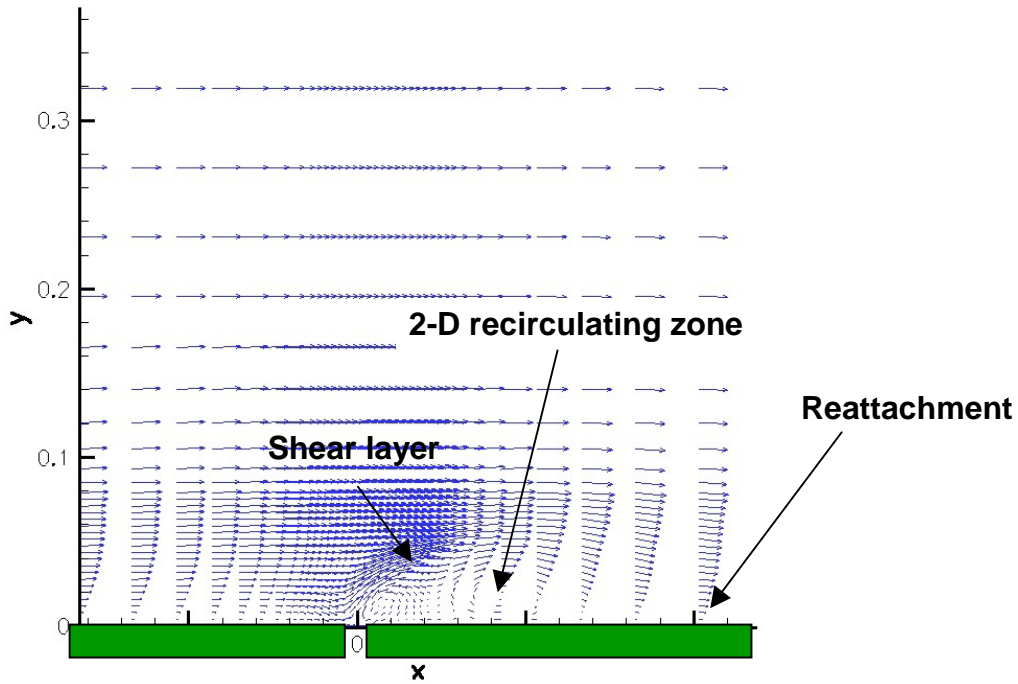


Figure 13. Example time-mean flow (zeroth-harmonic) near the slot, showing synthesized normal jet interacting with cross-flow and creating an apparent separation/reattachment region ($M = 1, J = 4$).

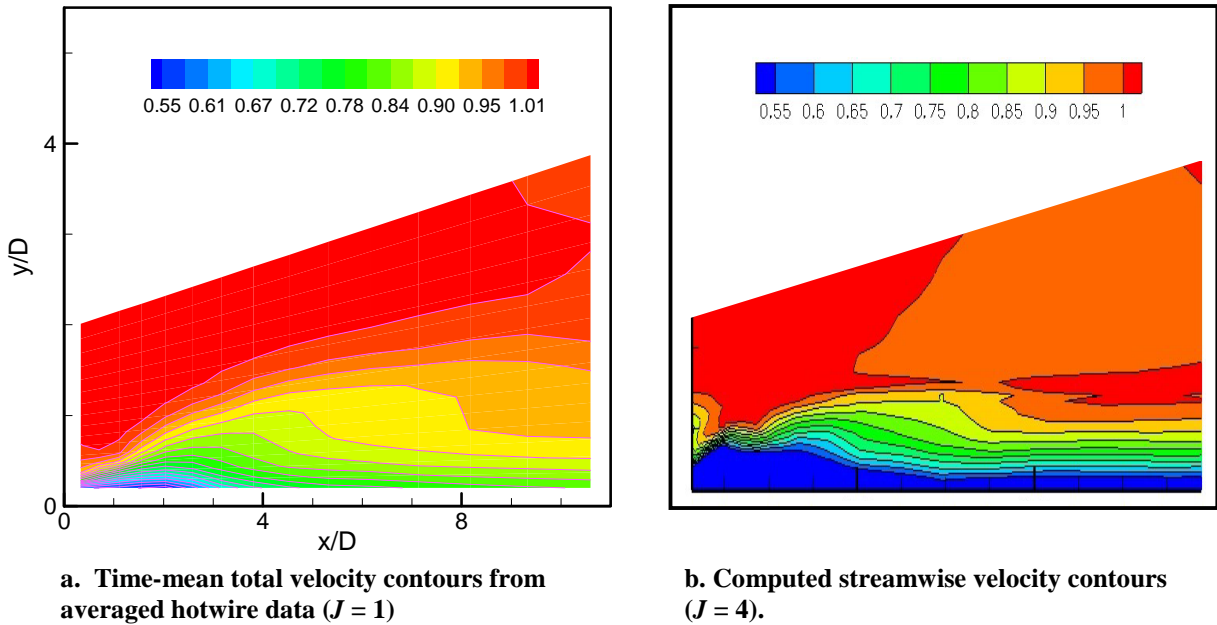


Figure 14. Comparison of computed and experimental time-mean velocity contours for normal synthetic jet with an 8:1 slot oriented normal to the cross-flow. The spatial coordinates are scaled to insure similarity. Note disparity between momentum ratios for experiment and computation.